Textile Research Journal

Short Communication

Textile Research Journal
2023, Vol. 93(19–20) 4656–4661

DOI: 10.1177/00405175231181089
journals.sagepub.com/home/trj
Sage

Experimental determination of in-plane permeability of nonwoven thin fibrous materials

Luwen Zhuang[1,2], S Majid Hassanizadeh[2,3] and Chao-Zhong Qin[4]

Abstract

Knowledge of hydraulic properties is crucial for understanding and modeling fluid flow in thin porous media. In this work, we have developed a new simple custom-built apparatus to measure the intrinsic permeability of a single thin fibrous sheet in the in-plane direction. The permeability was measured for two types of nonwoven thin fibrous porous materials using either the water or gas phase. For each layer, the measurements have been done for different combinations of flow direction and fiber orientation. The permeability values measured using gas and water were approximately close to each other. The permeability of the two samples was found to be anisotropic and the principal permeabilities were determined based on the measurements.

Keywords

Fibrous layer, fiber orientation, in-plane, permeability, thin porous media

In recent years, understanding and modeling of fluid flow in thin fibrous materials have received much attention due to the wide applications of thin fibrous materials.[1,2] The intrinsic permeability is one of the essential hydraulic properties to characterize flow and transport in thin fibrous materials (see, e.g., Spielman and Goren[3]). The intrinsic permeability is introduced in Darcy's law as follows:

$$\mathbf{q} = -\frac{\mathbf{k}}{\mu}\nabla P_w \tag{1}$$

where $\mathbf{q}$ is Darcy velocity or specific discharge, $\mathbf{k}$ is the intrinsic permeability, P_w denotes water pressure, and μ, ρ and g are fluid viscosity, fluid density and gravity acceleration, respectively. The intrinsic permeability represents the capability of a porous material to conduct fluids and is expected to be independent of fluid properties.

For most geological porous media (e.g. soils, rocks), the permeability is often measured by the constant head or falling head method.[4] However, the permeability of thin fibrous materials depends on the property of individual fibers as well as the arrangement of fibers.[5,6] Often, it has a tensorial nature; being different in different directions. Various empirical formulas have been proposed to calculate the permeability of fibrous materials accounting for orientation of fibers and homogeneity of the layer.[5] The formulas have been mainly derived based on solving the Navier–Stokes equation for flow around a single fiber or through periodic arrays of fibers. Also, some pore-scale simulations have been performed to investigate the influence of fiber orientation on the permeability of fibrous media.[6–8] Commonly, a three-dimensional (3D) unit cell of isotropic and/or oriented fibers with various fiber fractions is generated, the pore-scale flow is obtained numerically using the finite element method, and the cell permeability is calculated. Tamayol and Bahrami[8] have shown that fiber orientation has an influence on the permeability of most fibrous materials, with a more pronounced impact observed in materials with a porosity less than 0.7.

[1]School of Civil Engineering, Sun Yat-sen University, China
[2]Department of Earth Sciences, Utrecht University, The Netherlands
[3]Stuttgart Center for Simulation Science (SIMTECH), Stuttgart University, Germany
[4]State Key Laboratory of Coal Mine Disaster Dynamics and Control, Chongqing University, China

Corresponding author:
Luwen Zhuang, Zhuhai Campus, School of Civil Engineering, Sun Yat-sen University, 519082 Zhuhai, Guangdong, China.
Email: zhuanglw3@mail.sysu.edu.cn

Some experimental studies have been reported specific to quantifying the permeability of thin fibrous materials. Many studies have focused on measuring permeabilities for gas diffusion layers used in fuel cells[9,10] and polymer composites involved in resin transfer molding.[11,12] In most cases, these studies concerned the measurement of through-plane permeability.[13,14] The common technique is to measure gas pressure drop and flow rate perpendicular to the samples. Only a few studies have reported the measurements of in-plane permeability (see, e.g., Banerjee and Kandlikar[15] and Gostick et al.[16]). The in-plane permeability could be determined by the gas pressure difference and flow rate under general transverse flow or under radial flow. Most materials mentioned above are hydrophobic and the host fluid during the permeability measurements is often gas. The thickness of the gas diffusion layer in fuel cells is in the order of micrometers, whereas the thickness of fibrous layers in resin transfer molding is around millimeters. For thin fibrous materials, there is commonly a huge difference between the in-plane and through-plane permeability due to fiber orientation and differences in pore size distributions in different directions. Due to the anisotropy of thin fibrous materials and particularly due to their thinness, it is difficult to measure in-plane permeabilities experimentally. Recently, nonwoven materials have become popular in a wide range of industries due to their efficient manufacturing process and relatively low cost. Nonwoven materials are typically thin, whereas standard permeability measurement setups are not suitable for thin nonwoven porous layers. Also, to the best of our knowledge, there is no reliable experimental method for measuring the in-plane permeability of nonwoven thin fibrous materials.

For this study, we constructed a new simple custom-built setup to measure the in-plane permeability of a thin high-porosity nonwoven fibrous layer. Both water and gas were used as the injection fluid and two different types of thin fibrous absorbent tissue samples were used as the porous medium. The pressure drop and flow rate were measured during the experiments and permeability was calculated from equation (1).

Materials and methods

We employed two types of thin fibrous nonwoven sheets in this study, which are often used as absorbent tissues. The sample TY1 is rayon, which was an artificial deformable textile material that consisted of regenerated and purified cellulose. The sample TY2 was made of hydro-entangled pulp cellulose. The fibers were coated to prevent swelling. They were high-porosity sheets with nominal thicknesses being around 700 μm and average fiber radii of 10 μm. Properties of the two samples are shown in Table 1. Microscope images (Sigma 300, Zeiss, Germany) of the two sides of the samples are shown in Figure 1. On the front sides of both TY1 and TY2 samples we clearly see bundles of fibers running parallel to each other in one direction. On their back sides, however, we see mainly curved fibers with no preferred direction. This arrangement of fibers is expected to result in anisotropic behavior.

The original sample sheets were cut into strips with dimensions of 1 cm × 20 cm at 0, 45, or 90 degrees to the direction of fiber bundles (shown in Figure 1). The measurements were conducted in a custom-built setup, which is schematically presented in Figure 2. The experimental setup consisted of a 3D printed sample holder and a Plexiglass lid. The sample was placed in a groove of 1 × 20 cm created in the sample holder. The height of the groove was exactly equal to the nominal thickness of the fibrous sheet. The samples were put into water and saturated prior to the experiments and the deformation is neglected therefore. There was space reserved on the two ends of the sample to act as fluid inflow and outflow 'reservoirs' (see Figure 2). Silicon grease was applied to the surfaces of the groove and lid to prevent preferential flow along the contacting surfaces. Silicon glue was applied to the contact surfaces to make the setup airtight. The Plexiglas lid was mounted on the sample holder by screws. Pressure sensors (HMUM100; First Sensor, Germany) were inserted in the inlet and outlet tubes.

For the experiments using water, the setup and samples were degassed beforehand. Degassed and distilled water was used in the experiments. The water head at the inlet and outlet of the experimental setup were controlled. The water flow rate was measured volumetrically at the outlet. For experiments using gas (carbon dioxide (CO_2)), the inlet of the setup was connected to a flow controller to control the gas flow rate, and the outlet was connected to a flowmeter. During the experiments, the water or gas flow rate and the readings of the pressure sensors were recorded. Measurements have been taken for three individual strips of each material. All strips for each sample were taken from the same sheet. The experiments were conducted in a room with a constant temperature of 21 ± 0.5°C.

Table 1. Properties of the fibrous materials in this study

Parameter	TY1	TY2
Average fiber radius, r (μm)	10	10
Weight, W_f (g/m^2)	40	100
Layer thickness, D (μm)	705	724
Porosity, φ (–)	0.96	0.91

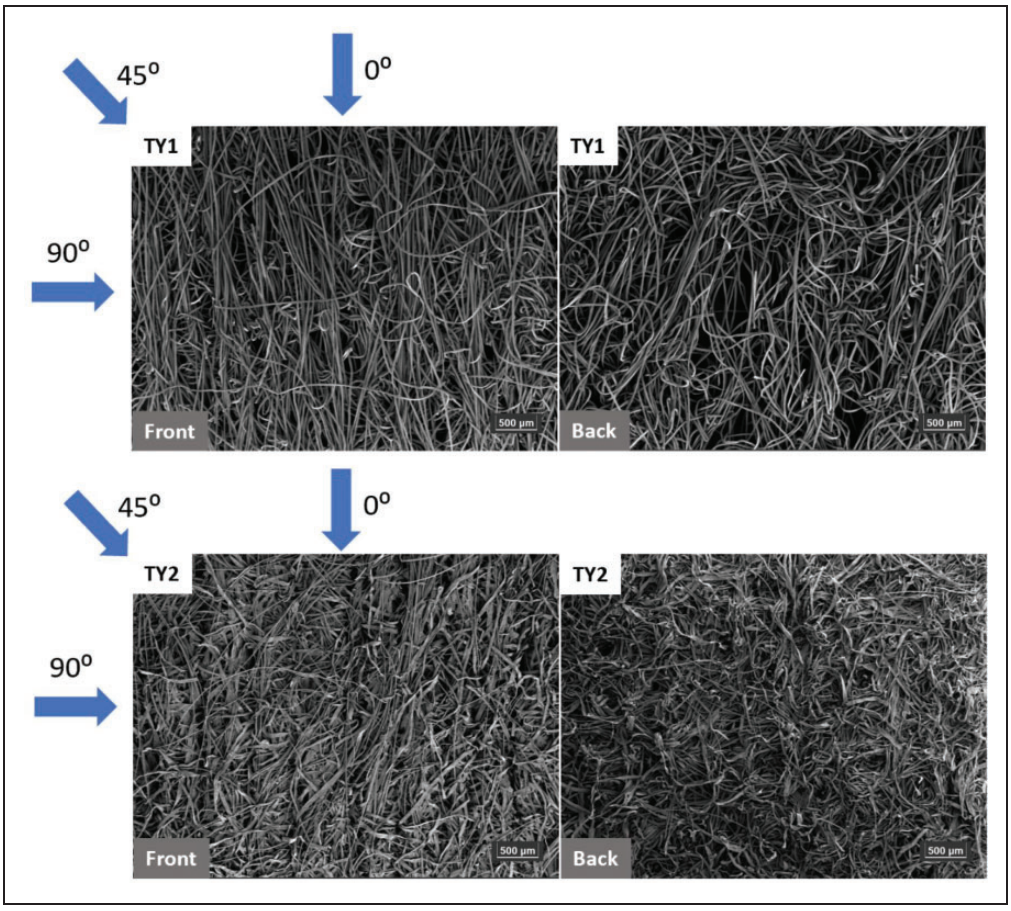

Figure 1. Microscope images of back and front sides of the two samples. The upper and lower rows of images are from samples TY1 and TY2, respectively. Blue arrows indicate flow directions during permeability measurements.

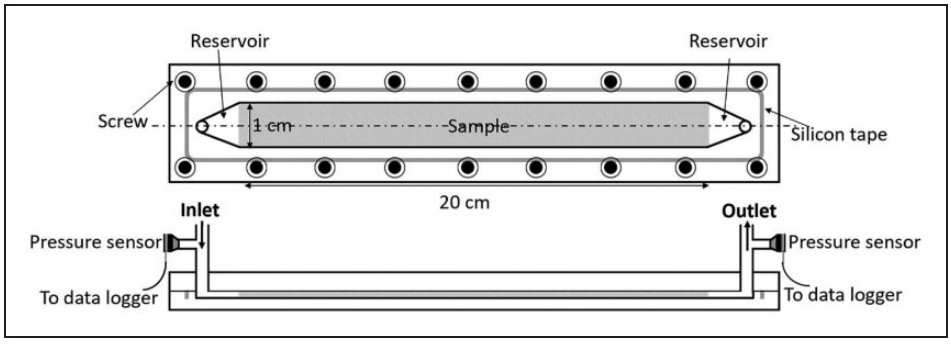

Figure 2. Schematic diagram of the experimental setup. The plan view and cutaway view are shown at the top and the bottom, respectively.

Results and discussion

As mentioned above, the samples were cut in three different angles with respect to the main direction of fiber bundles. So, we have got three test samples for each type of sample (TY1 and TY2). For each experiment, the water head difference or gas flow rate was chosen so as to ensure laminar flow in the samples. The resistance of the empty experimental setup was measured separately and was found to be very small. Figure 3 shows the measured velocity values versus pressure differences for water or gas phases. Error bars are also shown in the figure. In the case of measurements with water, the water head differences were controlled, and the measured velocity values were averaged for three repeated experiments. In the case of measurements with gas, the gas flow rate was controlled and the pressure

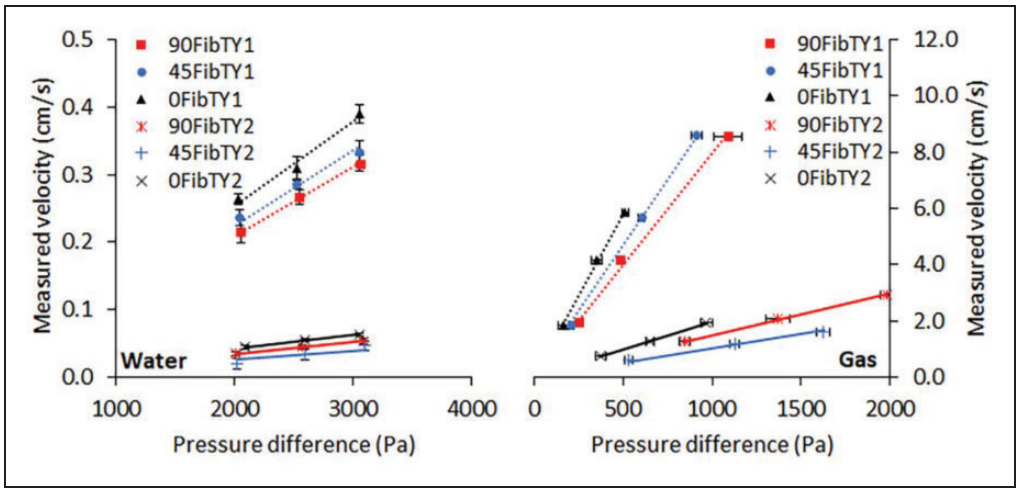

Figure 3. The measured velocities of water and gas in the samples versus various pressure differences (left figure for water and right figure for gas). Different samples of TY1 and TY2 sheets are labeled by the cutting angle.

differences were measured and average values for three repeated experiments were recorded.

For an incompressible fluid, in our case the water phase, we calculated the intrinsic permeability of the samples as follows:

$$k_w = \frac{\mu_w q_w L}{\Delta P_w} \tag{2}$$

where q_w is the water Darcy velocity, L is the length of the sample, that is, 20 cm, μ_w is water viscosity, and ΔP_w is the pressure drop along the sample. In the case of gas, in order to account for its compressibility and Klinkenberg effects, the following equation was employed to calculate permeability:[17]

$$k_g = \frac{2\mu_g L q_g}{({P_{in}}^2 - {P_{out}}^2)/P_{out}} \tag{3}$$

where μ_g is the viscosity of CO_2, q_g is gas velocity measured at the outlet, P_{in} and P_{out} are the pressures at the inlet and outlet, respectively. The resulting intrinsic permeability values are listed in Table 2. The largest permeability values were found in the direction parallel to the fiber bundle orientations for both samples TY1 and TY2. As expected, for all samples, the permeability values measured using gas and water are reasonably close to each other.

Also, we utilized the empirical formula proposed by Jackson and James[5] to calculate the permeability values of the two materials. The equation is expressed as follows:

$$k = \frac{3r^2}{20(1-\varphi)}(-\ln(1-\varphi) - 0.931) \tag{4}$$

Table 2. Calculated intrinsic permeability for different test samples

	Intrinsic permeability ($\times 10^{-10}$ m^2)	
Sample	Water	Gas
90FibTY1	2.08	1.71
45FibTY1	2.30	2.63
0FibTY1	2.53	2.67
90FibTY2	0.34	0.31
45FibTY2	0.25	0.23
0FibTY2	0.42	0.45

The calculated permeability values of TY1 and TY2 were found to be 8.57×10^{-10} and 2.46×10^{-10} m^2, respectively. Both measured and calculated values were of the same order of magnitude, with the calculated values being approximately three to four times larger than the measured values.

The different permeability values in three different in-plane directions indicate that the permeabilities of both samples TY1 and TY2 are anisotropic. For the in-plane directions, the anisotropic permeability is a two-dimensional (2D) tensorial quantity. For a 2D tensor, the principal values and directions can be determined based on measurements in at least three different directions. In our experiments, we measured permeability values in three directions that were at angles 0, 45°, and 90 degrees with respect to the fiber direction. These directions and the unknown principal directions of the permeability tensor are shown in Figure 4. The dashed lines are the two principal permeability directions, which are perpendicular to each other. The angle between the x axis and one of the principal directions

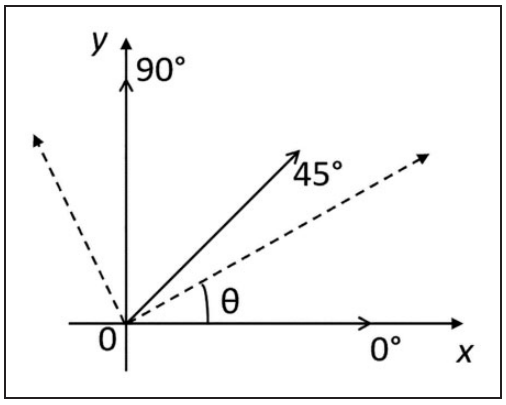

Figure 4. The schematic diagram of the principal permeability directions (dashed lines) and the directions in the experiments.

is shown as θ. We have calculated the principal permeability directions for the two samples. The detailed procedure can be found in Appendix 1. We found that the values of angle θ are 0° for TY1 and 54.5° for TY2. This means that the principal permeability values for TY1 are simply the values measured in the directions of 0 and 90 degrees. The principal permeability values for TY2 were calculated to be $2.4 \times 10^{-11}\,m^2$ and $5.2 \times 10^{-11}\,m^2$ in the directions of 54.5° and 144.5°. Similar experimental studies have been performed to determine the principal permeabilities in the liquid composite molding process.[12,18] Our experimental results have shown that the fiber bundle orientations influence the permeability of thin fibrous materials. This result has also been found in some numerical pore-scale simulations.[6,8]

Summary and conclusions

In this study, we have designed and constructed an experimental setup to measure the in-plane permeability of a thin high-porosity nonwoven fibrous layer. The permeabilities of two types of thin nonwoven materials were measured using either water or gas as the flowing fluid. The original sample sheets were cut into strips at 0, 45 or 90 degrees to the direction of fiber bundles. Our experimental results have shown that the fiber bundle orientations influence the permeability of thin fibrous materials. The principal permeabilities for the two samples have been calculated based on the experimental measurements. For sample TY1, the principal permeability directions are angles 0 and 90 degrees and permeability values given for TY1 in directions 0 and 90 degrees are the principal values. For sample TY2, the principal permeability direction values were calculated to be $2.4 \times 10^{-11}\,m^2$ and $5.2 \times 10^{-11}\,m^2$ and were at angles of 54.5° and 144.5° with respect to their fiber direction.

Declaration of conflicting interests

The author(s) declared no potential conflicts of interest with respect to the research, authorship, and/or publication of this article.

Funding

The author(s) disclosed receipt of the following financial support for the research, authorship, and/or publication of this article: The first author received funding from the National Natural Science Foundation of China (grant no. 42007165) and the Science and Technology Project in Guangzhou (grant no. 202102020222). The second author would like to thank the German Research Foundation for supporting this work by funding (EXC 2075–390740016) under Germany's Excellence Strategy to the Stuttgart Center for Simulation Science (SimTech) as well as the Deutsche Forschungsgemeinschaft (DFG; German Research Foundation) for supporting this work by funding SFB 1313, project number 327154368.

ORCID iD

Luwen Zhuang https://orcid.org/0000-0002-6300-9999

References

1. Prat M and Agaësse T. Thin porous media. In: V Kambiz (ed.) *Handbook of Porous Media*. London: Taylor & Francis, 2015, pp. 89–112.
2. Tavangarrad AH, Hassanizadeh SM, Rosati R, et al. Capillary pressure–saturation curves of thin hydrophilic fibrous layers: effects of overburden pressure, number of layers, and multiple imbibition–drainage cycles. *Text Res J* 2019; 89: 4906–4915.
3. Spielman L and Goren SL. Model for predicting pressure drop and filtration efficiency in fibrous media. *Environ Sci Technol* 1968; 2: 279–287.
4. Reynolds WD, Elrick DE, Youngs EG, et al. Saturated and field-saturated water flow parameters. In: JH Dane and G Topp (eds) *Methods of soil analysis. Part 4. Physical methods. SSSA Book Ser. 5. SSSA*. Madison, USA: Soil Science Society of America, 2002, pp. 797–801.
5. Jackson GW and James DF. The permeability of fibrous porous media. *Can J Chem Eng* 1986; 64: 364–374.
6. Stylianopoulos T, Yeckel A, Derby JJ, et al. Permeability calculations in three-dimensional isotropic and oriented fiber networks. *Phys Fluids* 2008; 20: 123601.
7. Tahir MA and Vahedi TH. Influence of fiber orientation on the transverse permeability of fibrous media. *Phys. Fluids* 2009; 21: 083604.
8. Tamayol A and Bahrami M. Transverse permeability of fibrous porous media. *Phys Rev E – Stat Nonlinear, Soft Matter Phys* 2011; 83: 1–9.
9. Feser JP, Prasad AK and Advani SG. Experimental characterization of in-plane permeability of gas diffusion layers. *J Power Sources* 2006; 162: 1226–1231.

10. Mukherjee M, Bonnet C and Lapicque F. Estimation of through-plane and in-plane gas permeability across gas diffusion layers (GDLs): comparison with equivalent permeability in bipolar plates and relation to fuel cell performance. *Int J Hydrog Energy* 2020; 45: 13428–13440.
11. Gebart BR and Lidström P. Measurement of in-plane permeability of anisotropic fiber reinforcements. *Polym Compos* 1996; 17: 43–51.
12. Weitzenböck JR, Shenoi RA and Wilson PA. Measurement of principal permeability with the channel flow experiment. *Polym Compos* 1998; 20: 321–335.
13. Mathias M, Roth J, Fleming J, et al. Diffusion media materials and characterisation. In: W Vielstich, A Lamm and Gasteiger HA (eds) *Handbook of Fuel Cells – Fundamentals, Technology and Application*. Chichester, UK: Wiley, 2003, pp. 517–537.
14. Orogbemi OM, Ingham DB, Ismail MS, et al. Through-plane gas permeability of gas diffusion layers and microporous layer: effects of carbon loading and sintering. *J Energy Inst* 2018; 91: 270–278.
15. Banerjee R and Kandlikar SG. Effect of temperature on the in-plane permeability in the gas diffusion layer of a PEM fuel cell. *ECS Trans* 2011; 41: 489–497.
16. Gostick JT, Fowler MW, Pritzker MD, et al. In-plane and through-plane gas permeability of carbon fiber electrode backing layers. *J Power Sources* 2006; 162: 228–238.
17. Tanikawa W and Shimamoto T. Comparison of Klinkenberg-corrected gas permeability and water permeability in sedimentary rocks. *Int J Rock Mech Min Sci* 2009; 46: 229–238.
18. Demaría C, Ruiz E and Trochu F. In-plane anisotropic permeability characterization of deformed woven fabrics by unidirectional injection. Part I: Experimental results. *Polym Compos* 2007; 28: 797–811.

Appendix 1: Calculations of principal permeability

The 2D permeability is a symmetric tensor as:

$$k = \begin{bmatrix} k_{xx} & k_{xy} \\ k_{xy} & k_{xy} \end{bmatrix} \tag{A1}$$

Darcy's law in two dimensions can be expressed as:

$$\begin{bmatrix} q_x \\ q_y \end{bmatrix} = -\frac{1}{\mu} \begin{bmatrix} k_{xx} & k_{xy} \\ k_{xy} & k_{yy} \end{bmatrix} \begin{bmatrix} \dfrac{\partial P_w}{\partial x} \\ \dfrac{\partial P_w}{\partial y} \end{bmatrix} \tag{A2}$$

For measurements at 0°, we had the conditions: $q_y = 0$, $\partial P_w/\partial y = 0$, and:

$$k_{m1} = -\frac{q_x \mu}{\partial P_w/\partial x} = k_{xx} + k_{xy} \tag{A3}$$

where k_{m1} is the measured permeability at 0°. For measurements at 90°, we had the conditions: $q_x = 0$, $\partial P_w/\partial x = 0$, and:

$$k_{m2} = -\frac{q_y \mu}{\partial P_w/\partial y} = k_{xy} + k_{yy} \tag{A4}$$

where k_{m2} is the measured permeability at 90°. For measurements at 45° counter-clockwise, the rotation of the coordinate system should be done in order to have flow on the x axis. The rotation-of-axis transformation can be defined as:

$$k' = \mathrm{A^T kA} \tag{A5}$$

where $\mathbf{k}'$ is the rotated permeability tensor, $\mathbf{A}$ and $\mathbf{A^T}$ are the rotation tensor and its transpose, respectively. The rotation tensor is:

$$\mathrm{A} = \begin{bmatrix} \cos\theta & -\sin\theta \\ \sin\theta & \cos\theta \end{bmatrix} \tag{A6}$$

where $\theta = 45°$ in this case. Darcy's law in this case can be written in terms of $\mathbf{k}'$:

$$\begin{bmatrix} q_{x'} \\ q_{y'} \end{bmatrix} = \frac{1}{\mu} \begin{bmatrix} k'_{xx} & k'_{xy} \\ k'_{xy} & k'_{yy} \end{bmatrix} \begin{bmatrix} \dfrac{\partial P_w}{\partial x'} \\ \dfrac{\partial P_w}{\partial y'} \end{bmatrix} \tag{A7}$$

Finally, we have:

$$k_{m3} = -\frac{q_{x'} \mu}{\partial P_w/\partial x'} = k_{xx} + k_{xy} \tag{A8}$$

where k_{m3} is the measured permeability at 45°. By solving the combination of equations (A3), (A4) and (A8), the 2D permeability tensor $\mathbf{k}$ was determined. We can find the principal permeability vectors by solving the characteristic equation.